

## Article

# Design Parameters Investigation on Sand Transportation Characteristics of V-Inclined Pipe Based on Eulerian–Eulerian Two-Phase Flow Model

Rao Yao <sup>1</sup>, Zhengwei Wang <sup>1,\*</sup> and Xingxing Huang <sup>2</sup><sup>1</sup> Department of Energy and Power Engineering, Tsinghua University, Beijing 100084, China<sup>2</sup> S.C.I. Energy, Future Energy Research Institute, Seidengasse 17, 8706 Zurich, Switzerland

\* Correspondence: wzw@mail.tsinghua.edu.cn

**Abstract:** During the operation of the water transportation pipelines in the upstream of the Yellow River, varying degrees of sand deposition often occur under a low flow rate. Taking into account the effect of different pipe inclinations, pipe diameters, and inlet sand content, the Eulerian–Eulerian two-phase model was applied in the numerical simulation of sediment-laden flow in a V-inclined pipe. The results indicate that there is a significant difference between a V-inclined pipe and horizontal pipe affected by gravity. Compared with the downward inclined pipe, sand deposition is evident in the upward inclined pipe. The high-velocity region moves upward and the asymmetry of the cross-sectional velocity increases. As the pipe diameter increases, the interaction between sand and the wall as well as the degree of turbulence decrease, so that the distribution of sand volume concentration across the cross section will be more uniform. Under different inlet sand content, the lowest point of the pipe experiences the most sand deposition, with sand volume concentration and velocity distribution across the cross-sections becoming uneven as inlet sand content increases. The location of the maximum liquid velocity varies from section to section. When the inlet sand content increases from 0.42% to 5% , the liquid velocity of the pipe cross-section no longer satisfies the rule of high velocity for middle and low velocity near the wall.



**Citation:** Yao, R.; Wang, Z.; Huang, X. Design Parameters Investigation on Sand Transportation Characteristics of V-Inclined Pipe Based on Eulerian–Eulerian Two-Phase Flow Model. *Water* **2023**, *15*, 4266. <https://doi.org/10.3390/w15244266>

Academic Editor: Giuseppe Bombino

Received: 22 November 2023

Revised: 7 December 2023

Accepted: 8 December 2023

Published: 13 December 2023



**Copyright:** © 2023 by the authors. Licensee MDPI, Basel, Switzerland. This article is an open access article distributed under the terms and conditions of the Creative Commons Attribution (CC BY) license (<https://creativecommons.org/licenses/by/4.0/>).

**Keywords:** inclined pipe; sediment-laden flow; sand transport characteristics; Eulerian–Eulerian two-phase model

## 1. Introduction

Due to the variation of flow rate and terrain undulation, there are different degrees of sand deposition when conveying sediment-laden flow. The entry of sand into the pipe increases the hydraulic loss. The movement speed of sand is obviously smaller than the flow rate, and often cannot be discharged outside the pipe. This leads to sand deposition easily occurring at the reverse slope and bending pipe section, which has a direct effect on the safety of the pipeline and the efficiency of sand transport [1,2]. The design parameters of pipe and sand are closely related to sand transport, so it is necessary to analyze the relationship between different design parameters and the sand transport characteristics in pipes. Studying the sand transport characteristics of the inclined pipe under different design parameters can provide accurate guidance for the design and operation of pipes, and enable effective anti-deposition management.

Pipeline transportation is widely used in the irrigation areas of the Yellow River because of its advantages of water saving and low cost [3]. However, the Yellow River is a natural river with high sediment content, and the suspended sediment is the main sediment source [4]. The problem of sand deposition has been restricting and hindering the development of irrigation. Current research on the sediment-laden flow of pipes focuses on the flow state [5–7], law of resistance loss [8,9], critical velocity [10,11], and wear of

pipes [12–14]. Based on experimental and theoretical studies of sediment-laden flow in pipes, many researchers have developed different empirical models for estimating different parameters, including pressure gradient, critical velocity, and wear rate. These prediction models obtain macroscopic parameters, which are simple to use, but only applicable to a certain range. Therefore, it is very important to accurately predict the sand transport characteristics in pipes.

The research methods that rely on empirical analysis and experimental studies do not reveal the essence of two-phase flow, while numerical simulation can quantitatively describe the changes in the flow field in time and space. More and more attention has been paid to the study of sand transport characteristics combined with numerical simulation. The Euler–Euler method finds frequent application in simulating flow containing sediment within pipes. In the study by Ekambara [15], ANSYS-CFX was employed for simulation. It was observed that the sand volume fraction distribution was well-replicated, and the forecasted frictional pressure drop closely matched the experimental data, thus confirming the numerical simulation's accuracy. In the numerical simulation conducted by Kaushal [16], the Mixture model and the Eulerian multiphase model were employed to simulate slurry flow characterized by a high concentration of fine particles. The findings demonstrated that the Eulerian multiphase model was better suited for accurately representing the changes in pressure drop and profiles of solids concentration. Yang [17], Li [18,19], and Zhang [20] used the Eulerian multiphase model to numerically simulate the sand transport characteristics of a pipe. They investigated the effects of pipe diameter, sand content, particle diameter, and flow rate on sand deposition in a horizontal pipe. Another method to simulate the sediment-laden flow is the Euler–Lagrange method. Xiong [21] and Capecelatro [22] conducted similar studies, with outcomes indicating that the Euler–Lagrange method adequately captures a more comprehensive description of sediment-laden flow in pipes, particularly when coarse particles are being transported. Lately, researchers have shown a growing interest in the CFD-DEM approach. Zhang [23], Januário [24], and others used CFD-DEM methods to study the sediment-laden flow of pipes, involving flow regimes and critical velocity. Nonetheless, the computational resource constraints restrict the applicability of such methods for analyzing slurries containing a high number of particles. On the basis of the above, the Eulerian–Eulerian two-phase model was used in this study.

At present, the study of sediment-laden flow in the inclined pipe by experiments and numerical simulation is relatively rare and mostly focuses on upward or downward inclined pipes. Liu [25] evaluated the influence of inclination and particle size on sediment-laden flow and found that sand deposition can also occur on the pipe wall under small inclinations, and small particles will lead to greater local sand volume concentrations and hydraulic gradients. Kesely [26] studied the influence of negative slope on critical velocity and carried out experimental research on different particle sizes. Matoušek [27–29] empirically established a mathematical and physical model for slurry flow in inclined pipes and conducted a comprehensive examination of the impact of pipe inclination, which revealed that the impact of pipe inclination on critical velocity is minimal when transporting coarse particles, but it cannot be disregarded when conveying fine particles. In an upward inclined pipe, an increase in inclination led to a reduction in both the degree of flow stratification and pressure drop. Conversely, the opposite trend was observed in a downward inclined pipe. There was a greater amount of deposition in the upward inclined pipe as opposed to the downward inclined pipe. Vlasak [30,31] conducted experiments and determined that the pressure drop in an upward inclined pipe was greater. Moreover, this discrepancy diminishes with higher flow rates and increased pipe inclination. Archibong-Eso [32] carried out experiments on horizontal and upward inclined pipes, and summarized the influence of flow rate, geometry, and particle parameters on critical velocity. Yang [33] employed the CFD-DEM method to simulate sediment-laden flow within the pipe and observed that the minimum value for transport capacity occurred within the range of 45° to 60°. Tebowei [34] investigated the sand transport characteristics of V-inclined pipes

utilizing the Eulerian multiphase model. It was observed that even a slight pipe inclination exerted a notable influence on sand transport characteristics, and deposition started to occur at higher velocities. These studies show that pipe inclination has an important influence on sand transport characteristics, and the long-distance water transportation pipelines will encounter unequal terrain undulation during the process of design, so the study of small angled V-inclined pipes is very important.

In this paper, the Eulerian–Eulerian two-phase model was used to conduct a numerical simulation of the sand transport characteristics of V-inclined pipes conveying sediment-laden flow were studied. The study analyzed the effect of pipe inclination, pipe diameter, and inlet sand content on the sand transport characteristics using the controlled variables method. The study is based on a typical V-inclined pipe utilized in an irrigation project for a 43.96 km pipeline along the Yellow River. Accurate prediction of sand transport characteristics is of great significance to the prevention of sand deposition in long-distance water transportation pipelines.

## 2. Mathematical Model

The research object of numerical simulation in this study is a three-dimensional V-inclined pipe, involving a solid–liquid two-phase flow. There are numerous models to describe two-phase flow. This study follows up on our previous study. The Eulerian–Eulerian two-phase model was considered. The mathematical model is the same as before, so the following formulas are consistent with our previous study [35].

### 2.1. Eulerian–Eulerian Two-Phase Model

In this model, each phase is treated as a continuous medium. The spatial distribution of the velocity and sand volume concentration is provided. This model has been widely used in simulating sediment-laden flow in pipelines [17,18,34]. In this model, the notion of phase volume fraction is incorporated. Different phases all satisfy the continuity equation and momentum equation.

The total volume fraction of each phase meets the following conditions:

$$\sum_{i=1}^n \alpha_i = 1 \tag{1}$$

$\alpha_i$  denotes the volume fraction of phase  $i$ . The subscripts  $s$  and  $l$  represent the solid and liquid phases, respectively.

In this study, it is assumed that there is no mass transfer between the solid particles and water. The continuity equation for phase  $i$  is expressed as follows:

$$\frac{\partial}{\partial t} (\alpha_i \rho_i) + \nabla \cdot (\alpha_i \rho_i \mathbf{v}_i) = 0 \tag{2}$$

where  $\mathbf{v}_i$  and  $\rho_i$  represent the velocity and physical density of phase  $i$ , respectively.

The interaction force between solid and liquid is considered, neglecting forces with weak effects, for instance, lift force and virtual mass force. Therefore, the momentum equation for phase  $i$  is:

$$\frac{\partial}{\partial t} (\alpha_i \rho_i \mathbf{v}_i) + \nabla \cdot (\alpha_i \rho_i \mathbf{v}_i \mathbf{v}_i) = -\alpha_i \nabla p + \nabla \cdot \bar{\tau}_i + \alpha_i \rho_i \mathbf{g} + \mathbf{R}_{ij} \tag{3}$$

$$\bar{\tau}_i = \alpha_i \mu_i \left( \nabla \mathbf{v}_i + \nabla \mathbf{v}_i^T \right) + \alpha_i \left( \lambda_i - \frac{2}{3} \mu_i \right) \nabla \cdot \mathbf{v}_i \bar{\mathbf{I}} \tag{4}$$

where  $\mathbf{g}$  represents gravitational acceleration,  $\bar{\tau}_i$  is the stress–strain tensor,  $\mu_i$  and  $\lambda_i$  are the shear and bulk viscosity,  $\bar{\mathbf{I}}$  denotes the unit tensor,  $\mathbf{R}_{ij}$  accounts for the interaction force between phases, and  $p$  stands for the pressure shared by each phase.

The Wen–Yu model is adopted as the interaction force model, which meets the requirements  $\mathbf{R}_{ls} = -\mathbf{R}_{sl}$ :

$$\mathbf{R}_{ls} = \frac{3\alpha_s\alpha_l\rho_l|\mathbf{v}_s - \mathbf{v}_l|}{4d_s} \alpha_l^{-2.65} \cdot \frac{24}{\alpha_l\text{Re}_f} \left[ 1 + 0.15(\alpha_l\text{Re}_f)^{0.687} \right] \cdot (\mathbf{v}_l - \mathbf{v}_s) \tag{5}$$

where,  $d_s$  represents the particle diameter, while  $\text{Re}_f$  stands for the relative Reynolds number.

### 2.2. Turbulence Model

This study utilized the mixture  $k - \varepsilon$  turbulence model, which strikes a balance between computational efficiency and accuracy. This model relies on mixture properties to capture crucial turbulent characteristics. The values of  $k$  and  $\varepsilon$  can be determined from the following equations:

$$\frac{\partial}{\partial t}(\rho_m k) + \nabla \cdot (\rho_m \mathbf{v}_m k) = \nabla \cdot \left( \left( \mu_m + \frac{\mu_{t,m}}{\sigma_k} \right) \nabla k \right) + G_{k,m} - \rho_m \varepsilon \tag{6}$$

$$\frac{\partial}{\partial t}(\rho_m \varepsilon) + \nabla \cdot (\rho_m \mathbf{v}_m \varepsilon) = \nabla \cdot \left( \left( \mu_m + \frac{\mu_{t,m}}{\sigma_\varepsilon} \right) \nabla \varepsilon \right) + \frac{\varepsilon}{k} (C_{1\varepsilon} G_{k,m} - C_{2\varepsilon} \rho_m \varepsilon) \tag{7}$$

In the given equations,  $k$  represents the turbulent kinetic energy,  $\varepsilon$  stands for the vortex dissipation rate, and  $\sigma_k$  and  $\sigma_\varepsilon$  denote the Prandtl numbers for  $k$  and  $\varepsilon$ , respectively.  $C_{1\varepsilon}$  and  $C_{2\varepsilon}$  are constants, while  $G_{k,m}$  represents the generation of turbulence kinetic energy, and  $\mu_{t,m}$  stands for the turbulent viscosity for the mixture.

$$G_{k,m} = \mu_{t,m} \left( \nabla \mathbf{v}_m + (\nabla \mathbf{v}_m)^T \right) : \nabla \mathbf{v}_m \tag{8}$$

$$\mu_{t,m} = \rho_m C_\mu \frac{k^2}{\varepsilon} \tag{9}$$

where  $C_\mu$  represents a constant.  $\rho_m$ ,  $\mathbf{v}_m$ , and  $\mu_m$  stand for the mixture density, mixture velocity, and mixture molecular viscosity, respectively.

$$\rho_m = \sum_{i=1}^n \alpha_i \rho_i \tag{10}$$

$$\mathbf{v}_m = \frac{\sum_{i=1}^n \alpha_i \rho_i \mathbf{v}_i}{\sum_{i=1}^n \alpha_i \rho_i} \tag{11}$$

$$\mu_m = \sum_{i=1}^n \alpha_i \mu_i \tag{12}$$

## 3. Simulation Method

### 3.1. Physical Model

The physical model is based on a typical V-inclined pipe utilized in an irrigation project along the Yellow River. This configuration comprises a downward inclined pipe with a negative inclination and an upward inclined pipe with a positive inclination. The pipe length investigated in this paper is 80m. Five cross-sections, labeled as S1, S2, S3, S4, and S5, have been selected along the pipe, with S3 being the cross section at which the pipe is at its lowest. S1, S2, S4, and S5 are positioned at distances of  $-20$  m,  $-10$  m,  $10$  m, and  $20$  m from S3, respectively.

### 3.2. Grid Independent Test

The computational domain is the fluid domain of the V-inclined pipe. The model in Figure 1 is taken as an example to illustrate the grid independence verification. Considering that sand deposition occurs at the pipe wall, the boundary layer of the grid was refined with five layers. The first boundary layer had a height of 5 mm and a growth rate of 1.2, as shown in Figure 2. Different grid numbers of 764,000, 1,487,600, and 1,855,600 were used to verify the grid independence. The slurry velocity of S3 was used as the evaluation parameter. At the inlet, sand volume concentration was specified as 0.42% and inflow velocity was established at 0.3 m/s. Comparisons are shown in Figure 3. It can be found that when the grid number is greater than 1,487,600, the variation of slurry velocity is less than 0.03%, so finally the grid number of 1,487,600 was chosen for the final numerical simulation.

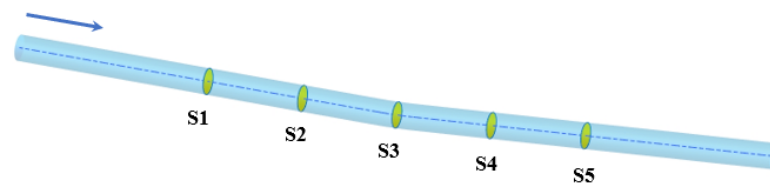


**Figure 1.** Physical model of V-inclined pipe ( $D = 2600$  mm,  $\theta = \pm 2^\circ$ ).

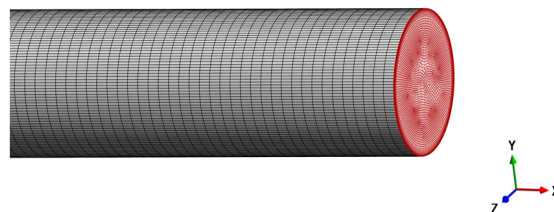


**Figure 2.** Mesh of the V-inclined pipe.

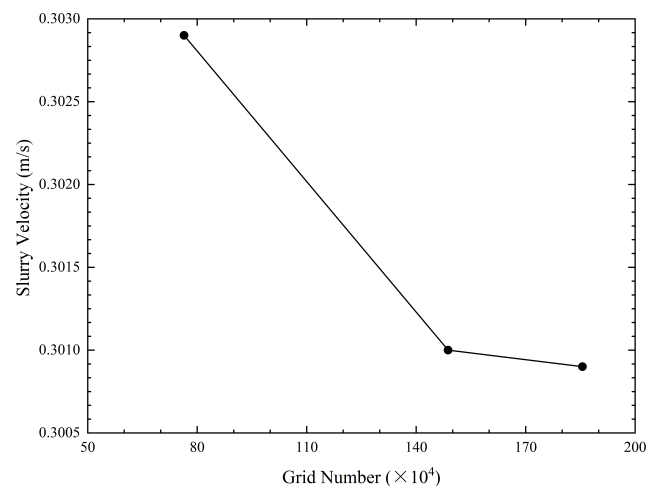


**Figure 3.** Slurry velocity under different grid numbers.

### 3.3. Solution Techniques

ANSYS Fluent was chosen to carry out related work. A velocity boundary condition was implemented at the inlet, while a pressure boundary condition was implemented at the outlet. The wall surfaces adopted a no-slip wall condition.

The primary phase is water, while the secondary phase is sand. Water was considered to be an incompressible fluid. Phase transformation was not taken into account, thus the physical properties of water and sand were treated as constant. Solid particles were treated as spheres of the same particle size. It is proved by experiments that the bed roughness has

no obvious influence when transporting fine particles compared with coarse gravel [36]. Due to the number of fine particles in the Yellow River, the effect of pipe roughness was not considered.

In the research of sediment-laden flow in pipelines, critical velocity and sand transport characteristics are mostly studied. Numerical simulations of both are essentially performed for solid–liquid two-phase flow, but the research content is different. The critical velocity of sediment-laden flow is the macroscopic condition, which is mostly determined by the empirical formula. However, sand transport characteristics are a microscopic condition. The previous study [35] employed both numerical simulation and empirical formulas to predict the critical velocity. The comparative results validated the accuracy of numerical simulation for solid–liquid two-phase flow, thus obviating the need for repetition in this paper.

#### 4. Results and Discussion

The sand transport characteristics have a close relationship with pipe inclination, pipe diameter, and inlet sand content. Building upon the findings [17–20] from the horizontal pipe study, the distribution law of sediment-laden flow in V-inclined pipes was analyzed under varying parameters using the controlled variables method.

##### 4.1. Pipe Inclination

Critical velocity within the range of  $-1.35^\circ \pm 5^\circ$  has been demonstrated to be minimally affected by pipe inclination. However, it has been observed that the sand transport characteristics are indeed influenced by pipe inclination [37–39]. Compared with horizontal pipes, pipe inclination exacerbates the complexity of the multiphase flow. In particular, small angled inclination often has an important effect on sand transport characteristics. The simulated pipe inclinations were selected to be  $\pm 2^\circ$ ,  $\pm 4^\circ$ , and  $\pm 6^\circ$ , respectively. Table 1 shows parameters under different pipe inclinations. The inlet sand content was given by uniform distribution. The inflow velocity was 0.3 m/s.

**Table 1.** Parameters for numerical simulation under different pipe inclinations.

Parameters	V-Inclined Pipe	Horizontal Pipe
Pipe inclination	$\pm 2^\circ, \pm 4^\circ, \pm 6^\circ$	\
Pipe length	80 m	80 m
Pipe diameter	2600 mm	2600 mm
Liquid density	$998.2 \text{ kg} \cdot \text{m}^{-3}$	$998.2 \text{ kg} \cdot \text{m}^{-3}$
Solid density	$2300 \text{ kg} \cdot \text{m}^{-3}$	$2300 \text{ kg} \cdot \text{m}^{-3}$
Particle size	0.02 mm	0.02 mm
Inlet sand content	0.42%	0.42%

Figures 4–6 are the contours of the sand volume concentration contours and the turbulent kinetic energy of the pipe cross-section at different pipe inclinations. A small angled V-inclined pipe is affected by gravity and has different sand transport characteristics from a horizontal pipe. At the same inflow velocity, sand deposition of a horizontal pipe is less than that of the V-inclined pipe. The distribution of sand volume concentrations at different cross-sections is uneven and asymmetrical in the V-inclined pipe. S3 is the cross-section where the most sand deposition occurs. The majority of the sand was concentrated in the upward inclined section of the pipe. This is because the component force of particle gravity parallel to the pipe centerline changes with the pipe inclination. A large portion of the resistance is offset by the gravity component in the downward inclined pipe, while in the upward inclined pipe, it inhibits the flow even more.

Additionally, it has been observed that sand deposition increases with the elevation of pipe inclination. The maximum sand volume concentrations at  $\pm 2^\circ$ ,  $\pm 4^\circ$ , and  $\pm 6^\circ$  pipe inclinations are 34.7%, 21.4%, and 19.5%, respectively. The maximum sand volume concentration in the cross-section gradually decreases with the increase in pipe inclination,

as shown in Table 2. This is attributed to the fact that as the pipe inclines towards the vertical position from a horizontal position, the settling effect of particles will be weakened and the symmetry of the sand volume concentration will be improved in the cross-sections.

In the V-inclined pipe, the distribution of cross-sectional turbulent kinetic energy is also characterized by unevenness and asymmetry. Above the cross-section, the turbulent kinetic energy is higher in the upward inclined pipe. Conversely, below the cross-section, the turbulent kinetic energy is higher in the downward inclined pipe. The reason is that part of the sand will flow back to the bottom of the pipe because of the liquid shedding process and sand deposition, resulting in a significant difference in sand transport characteristics between upward and downward inclined pipes.

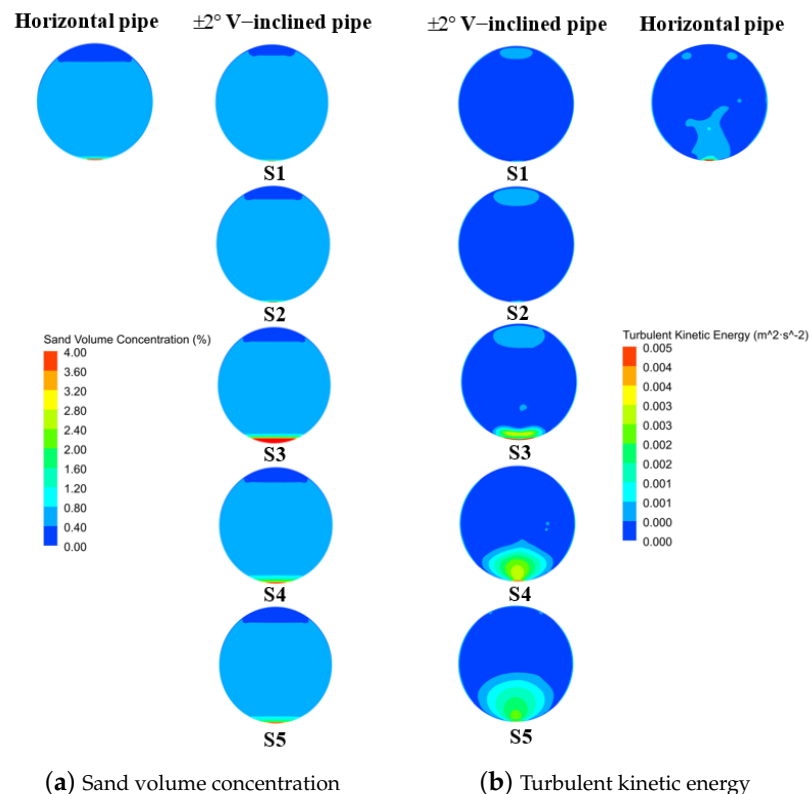


Figure 4. Contours of pipe cross-section at  $\pm 2^\circ$  V-inclined pipe.

Table 2. Maximum cross-sectional sand volume concentration under different pipe inclinations.

	S1	S2	S3	S4	S5
$\pm 2^\circ$	8.3%	11.7%	34.7%	23.1%	13.1%
$\pm 4^\circ$	3.6%	5.1%	21.4%	13.6%	10.9%
$\pm 6^\circ$	3.2%	4.4%	19.5%	10.8%	8.6%

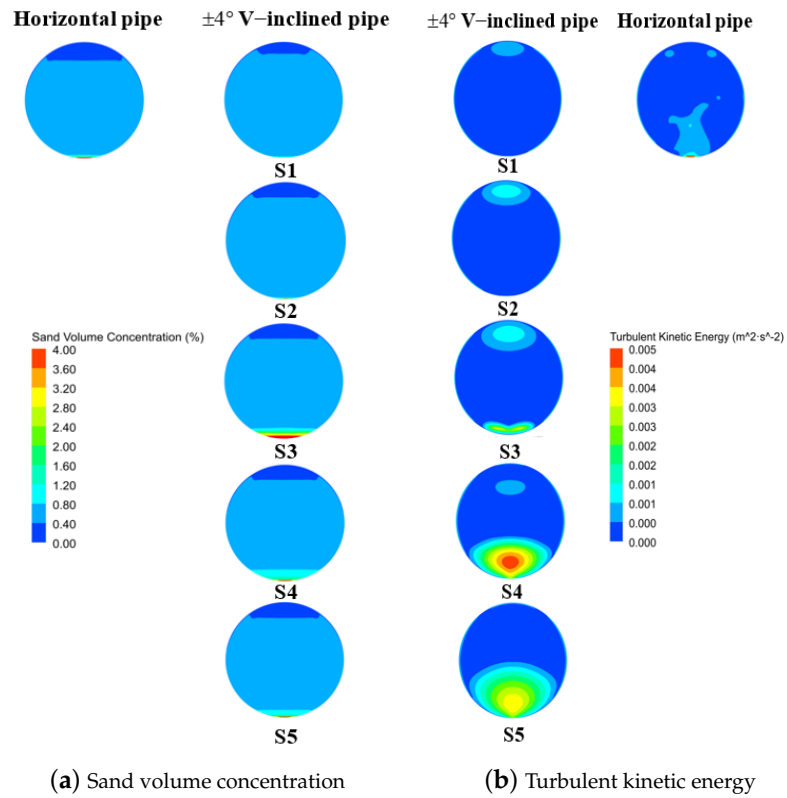


Figure 5. Contours of pipe cross-section at  $\pm 4^\circ$  V-inclined pipe.

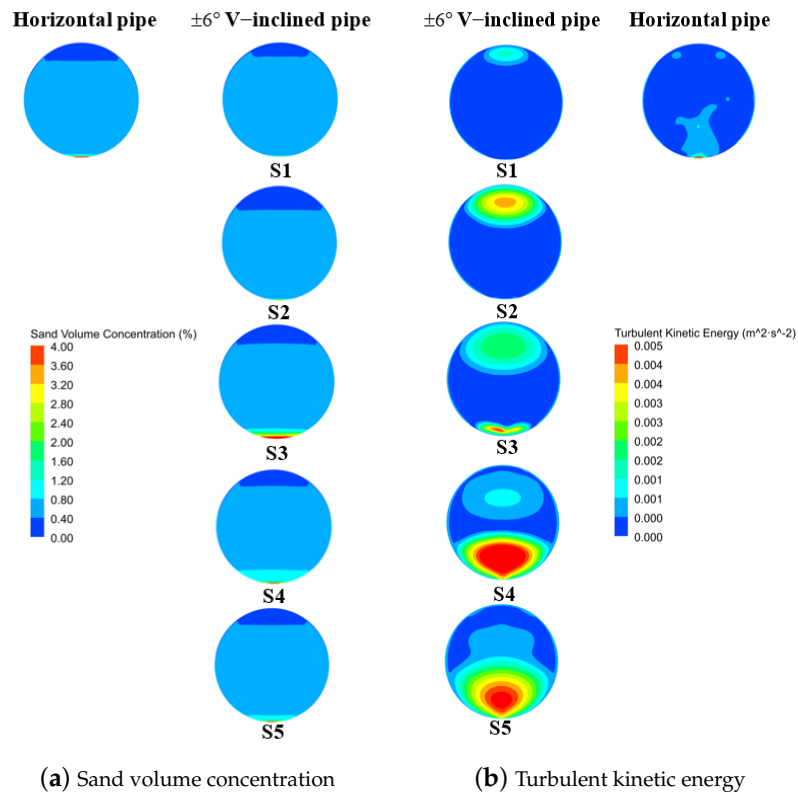


Figure 6. Contours of pipe cross-section at  $\pm 6^\circ$  V-inclined pipe.

#### 4.2. Pipe Diameter

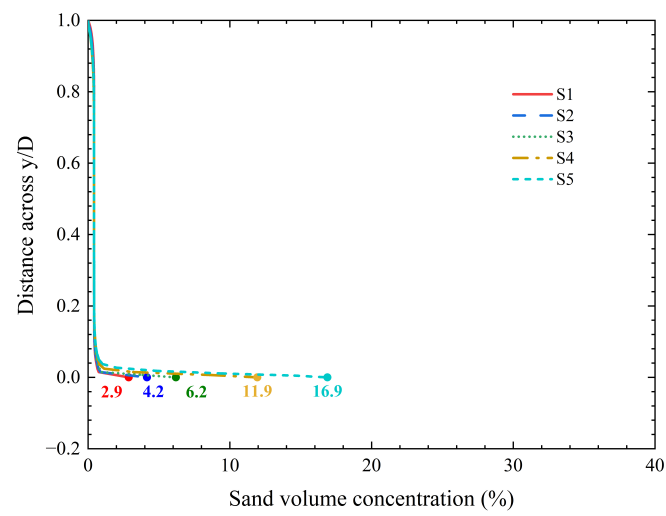
The simulated pipe diameters were selected to be 2600 mm, 1600 mm, and 1200 mm, respectively. Table 3 shows the parameters under different pipe diameters. The inlet sand content was given by uniform distribution. The inflow velocity was 0.3 m/s.

**Table 3.** Parameters for numerical simulation under different pipe diameters.

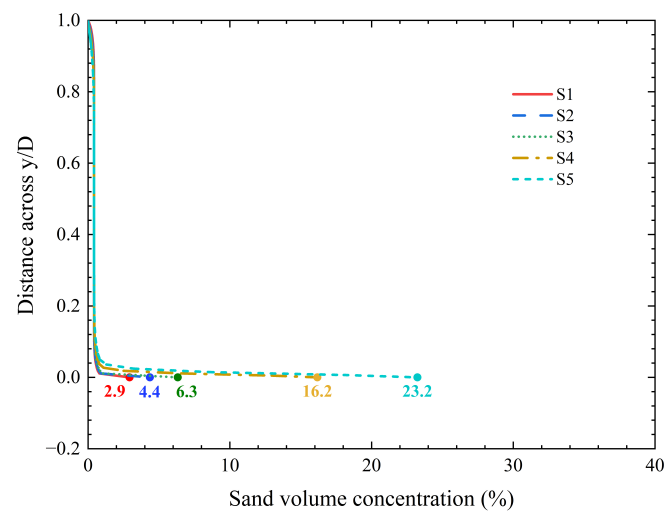
Parameters	V-Inclined Pipe
Pipe inclination	$\pm 2^\circ$
Pipe length	80 m
Pipe diameter	1200 mm, 1600 mm, 2600 mm
Liquid density	$998.2 \text{ kg} \cdot \text{m}^{-3}$
Solid density	$2300 \text{ kg} \cdot \text{m}^{-3}$
Particle size	0.02 mm
Inlet sand content	0.42%

The vertical distribution law of concentration is a fundamental topic in the investigation of sand transport characteristics. The simulation obtained the vertical distribution of sand volume concentration at different pipe diameters, as shown in Figure 7. It can be seen that after a certain distance of flow, the vertical distribution of cross-sectional sand volume concentration is not uniform under different pipe diameters, forming a distribution pattern with small sand volume concentrations at the upper cross-section and large sand volume concentrations at the lower cross-section. At this time, the flow in the pipe belongs to the non-homogeneous flow with the promoted layer, which is related to the selection of the inlet velocity near the critical velocity. At the critical velocity, the turbulent kinetic energy is just unable to maintain the suspended motion of solid particles, and the sand will not accumulate in piles, although it is slowly pushing forward at the bottom of the pipe.

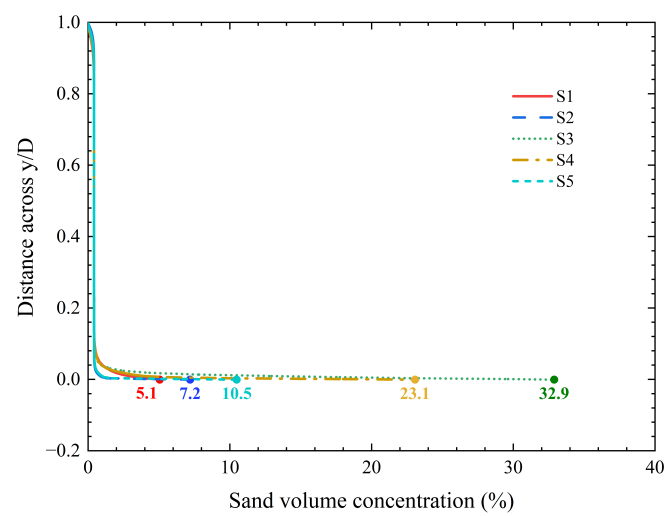
Combined with Figures 7 and 8, it was found that the inhomogeneity of the vertical distribution of the sand volume concentration decreased with the increase in pipe diameter. This can be attributed to the weakened interaction between solid particles and the wall, as well as the spatial release effect. The maximum sand volume concentration in the cross-section increases as the pipe diameter increases under the same inlet sand content and velocity, but the location where the maximum sand volume concentration appears is not the same. For the small pipe diameters of 1200 mm and 1600 mm, sand volume concentration at the bottom of the cross-section gradually increases as the flow distance increases. However, in the case of the larger pipe diameter of 2600 mm, it is largest at the lowest point of the V-inclined pipe. From Figure 9, on the one hand, the particle spacing is larger after the pipe diameter increases, and the turbulent pulsation of particles is not enough to cause a high frequency of particle collision and extrusion; on the other hand, the influence brought by pipe inclination makes a certain degree of backflow in the upward inclined pipe and the speed of the backflow increases with the augmentation in pipe diameter.



(a) D = 1200 mm



(b) D = 1600 mm



(c) D = 2600 mm

Figure 7. Vertical distributions of sand volume concentration at different pipe diameters.

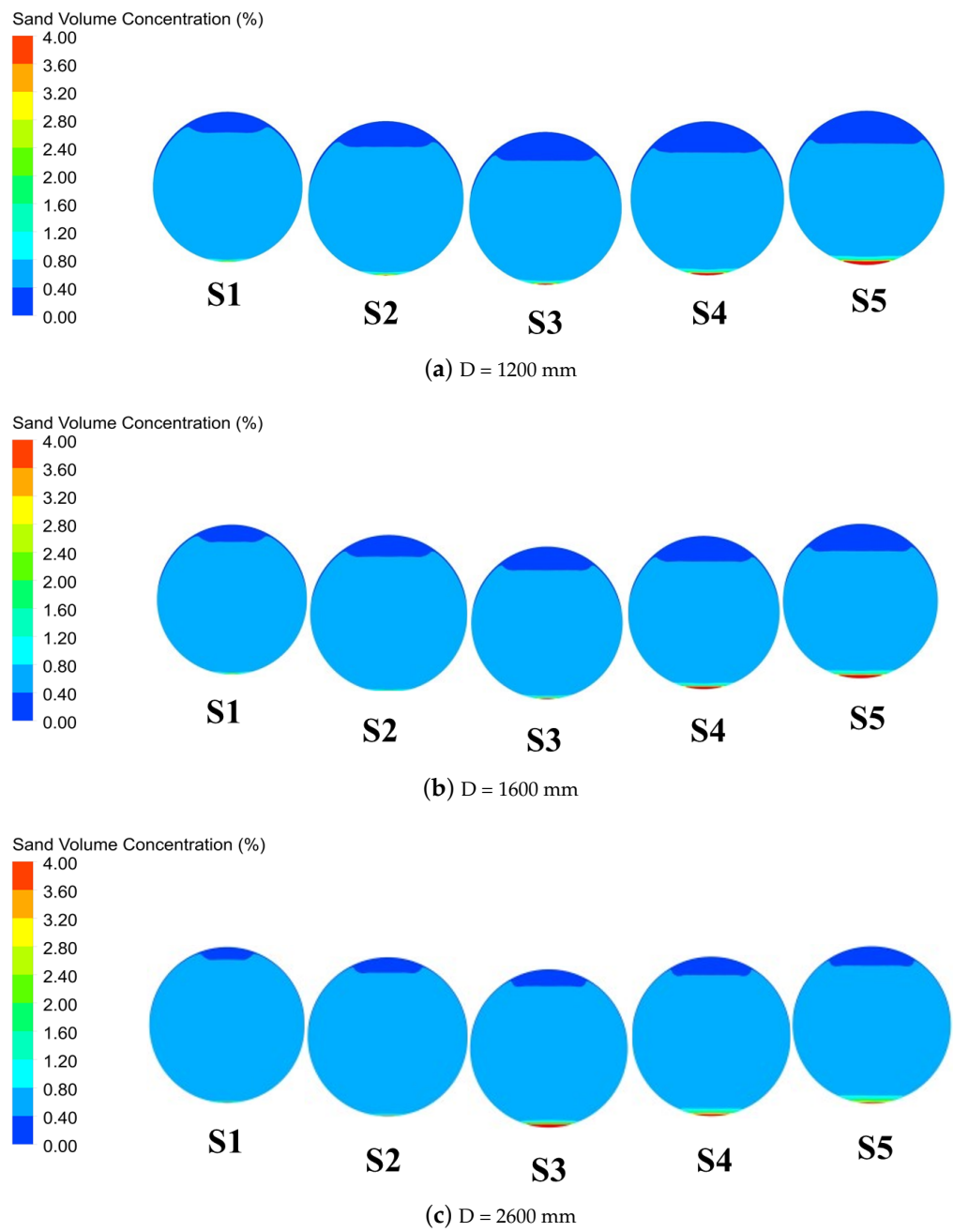


**Figure 8.** Sand volume concentration contours of pipe cross-section at different pipe diameters.

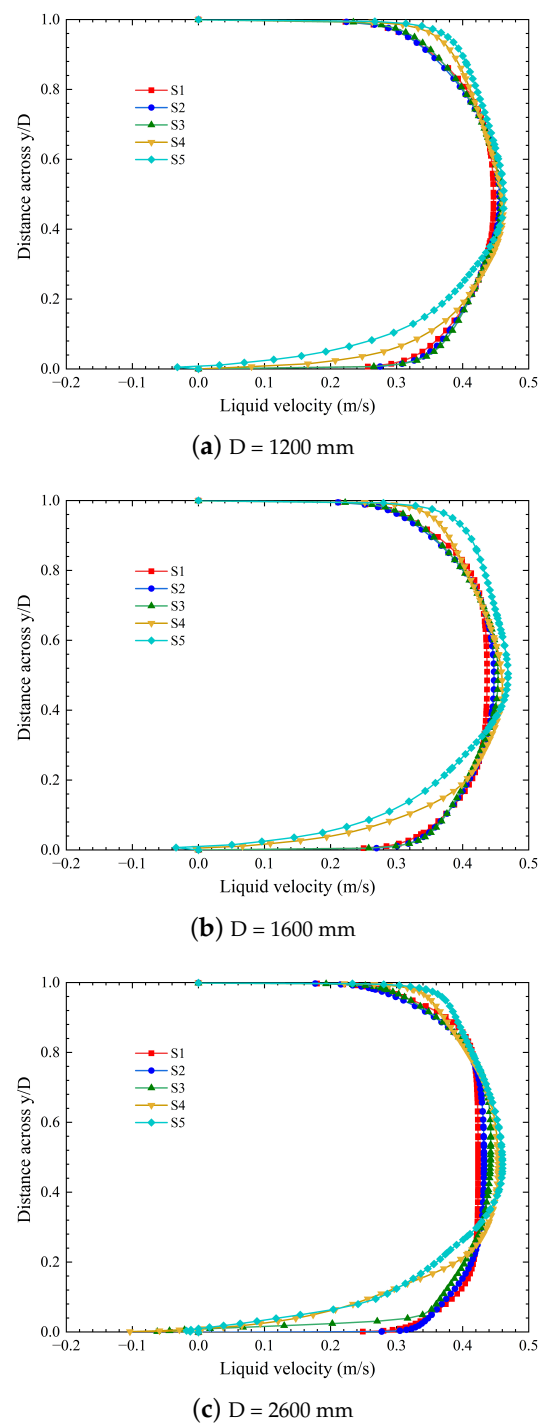


**Figure 9.** Liquid velocity distribution of pipe cross-section at different pipe diameters.

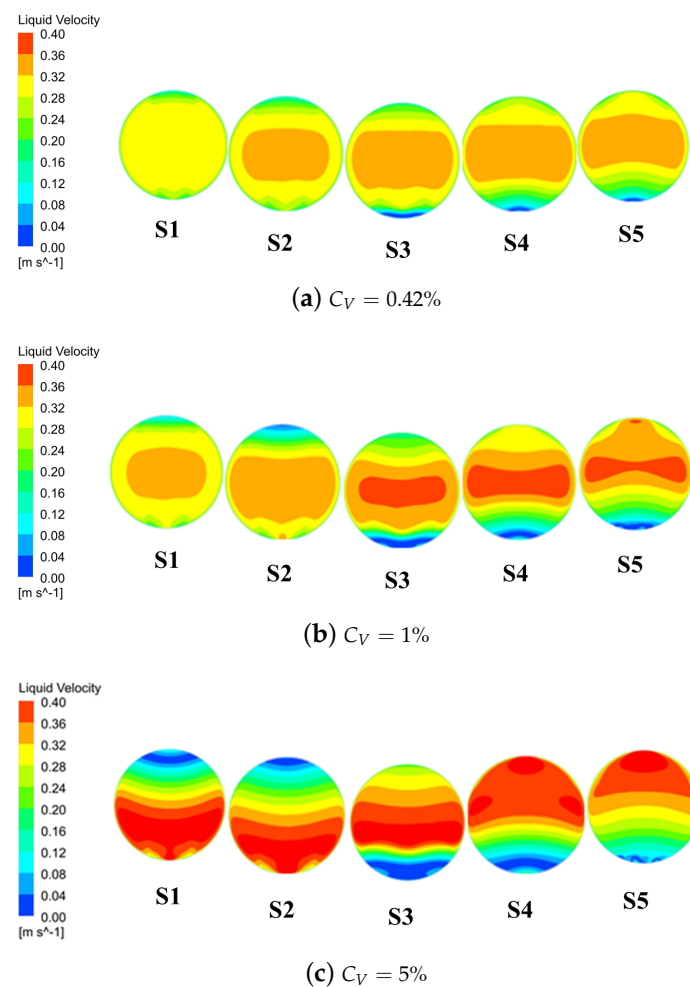
#### 4.3. Inlet Sand Content

The sand content of rivers is constantly changing due to seasonal changes. The inlet sand content has an effect on the sand transport characteristics of the pipe, so numerical simulations were performed at three different inlet sand contents, 0.42%, 1%, and 5%, respectively. Table 4 shows parameters under different inlet sand contents. The inlet sand content was given by uniform distribution. The inflow velocity was 0.3 m/s.

**Table 4.** Parameters for numerical simulation under different inlet sand contents.

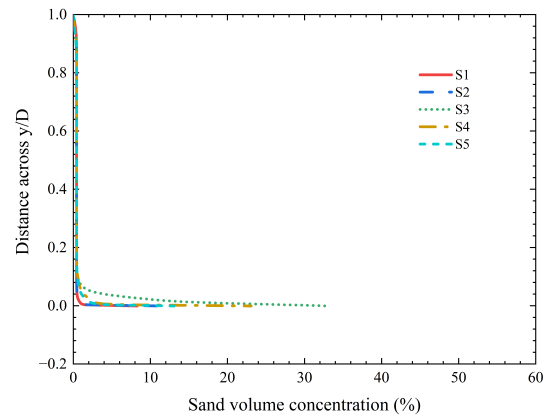
Parameters	V-Inclined Pipe
Pipe inclination	$\pm 2^\circ$
Pipe length	80 m
Pipe diameter	2600 mm
Liquid density	$998.2 \text{ kg} \cdot \text{m}^{-3}$
Solid density	$2300 \text{ kg} \cdot \text{m}^{-3}$
Particle size	0.02 mm
Inlet sand content	0.42%, 1%, 5%

Figure 10 illustrates the contours of liquid velocity distribution at various cross-sections with varying inlet sand contents. It can be observed that, in comparison to the downward inclined pipe, a distinct low-speed zone emerges at the bottom of the upward inclined pipe. This can be attributed to the sand deposition at the bottom of the pipe. Among the chosen cross-sections, S3 exhibits the widest range of low-speed zones. The non-uniformity in liquid velocity distribution at a given inflow velocity rises with an increase in inlet sand content. Specifically, when the inlet sand content is at 0.42% and 1%, the highest liquid velocity occurs at the center of the cross-section. However, when the inlet sand content of the pipe is 5%, the position of the maximum liquid velocity has different performance in different cross-sections, which is due to the increased interaction of particles movements caused by the increased inlet sand content.

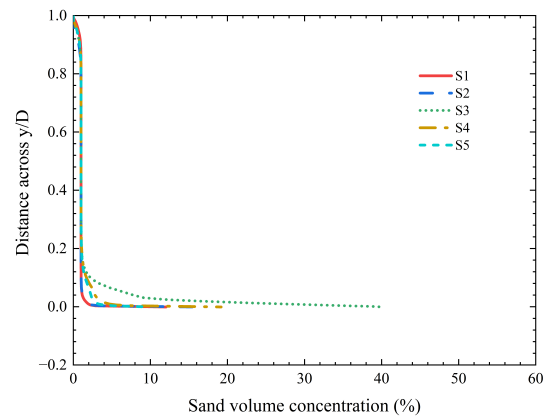


**Figure 10.** Liquid velocity contours of the pipe cross-section.

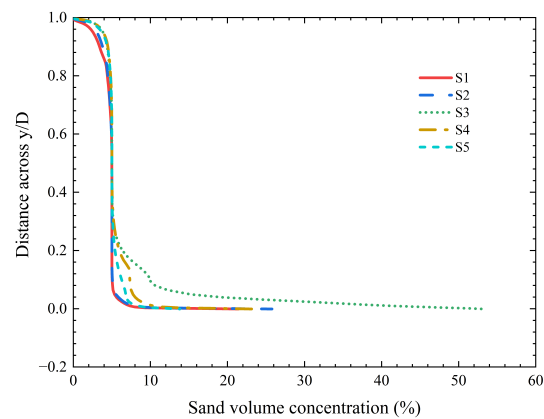
Figure 11 depicts the distribution of sand volume concentration in the cross-sections with varying inlet sand contents. Notably, the sand volume concentration in the selected cross-sections reaches its peak in S3. As the inlet sand content increases, the sand volume concentration at the bottom of the pipe rises, and the thickness of sand deposition also expands. This phenomenon is closely linked to the distribution of low-speed zones.



(a)  $C_V = 0.42$



(b)  $C_V = 1$



(c)  $C_V = 5$

Figure 11. Sand volume concentration distribution of the pipe cross-section.

### 5. Conclusions

The Eulerian–Eulerian two-phase model was used to predict the sand transport characteristics in the V-inclined pipe, including  $\pm 2^\circ$ ,  $\pm 4^\circ$ , and  $\pm 6^\circ$ . The findings indicate a notable disparity in sand transport characteristics between the horizontal and V-inclined

pipes, particularly at low flow rates. In the same cross-section, the distribution of sand in the horizontal direction is nearly symmetrical, but the vertical distribution is uneven and asymmetrical, with the high-velocity area moving upward and the asymmetry of the cross-sectional velocity increasing. The effects of pipeline inclination, pipeline diameter, and inlet sand content on sand transport characteristics were also studied, and the results showed that:

(1) Pipe inclination exerts a discernible influence on sand transport in small angled V-inclined pipes. The sand volume concentration in the upward inclined pipe surpasses that in the downward inclined pipe. The maximum sand volume concentration at  $\pm 2^\circ$ ,  $\pm 4^\circ$ , and  $\pm 6^\circ$  pipe inclinations are 34.7%, 21.4%, and 19.5%, respectively. The maximum sand volume concentration in the cross-section gradually decreases with the increase in pipe inclination. This is attributed to some solid particles being redirected back towards the bottom of the pipe due to the influence of the liquid phase shedding process and the component force of particle gravity. The emergence of this backflow phenomenon results in a notable alteration in sand transport characteristics.

(2) When the pipe diameter increases, the interaction between solid particles and the wall as well as the degree of turbulence decrease. This results in a more even distribution of sand volume concentration across the pipe cross-section. However, the point where the highest sand concentration occurs is not consistent. The highest sand concentration occurs at the upward inclined pipe when the pipe diameter is 1200 mm and 1600 mm, but at the lowest section S3 of the pipe when the pipe diameter is 2600 mm.

(3) At a certain flow rate, the pipe's lowest point experiences the most sand deposition. Under a specific flow rate, the lowest point of the pipe accumulates the highest amount of sand. The disparity in sand volume concentration and liquid velocity distribution becomes more pronounced as the inlet sand content increases. When the inlet sand content increases from 0.42% to 5%, the liquid velocity of the pipe cross-section no longer satisfies the rule of high velocity for the middle and low velocity near the wall.

In future studies, we will consider large-angled V-inclined pipe in the physical model, and comprehensively consider the interaction between solid and liquid phases in the mathematical model, so as to deeply explore the influence of pipe inclination on critical velocity and sand transportation characteristics.

**Author Contributions:** Conceptualization, R.Y.; methodology, R.Y.; software, R.Y.; validation, X.H.; formal analysis, R.Y.; investigation, R.Y.; resources, R.Y.; writing—original draft preparation, R.Y.; writing—review and editing, X.H., Z.W. All authors have read and agreed to the published version of the manuscript.

**Funding:** This research received no external funding.

**Data Availability Statement:** Data are contained within the article.

**Conflicts of Interest:** The authors declare no conflict of interest.

## Abbreviations

The following abbreviations are used in this manuscript:

CFD    computational fluid dynamics  
DEM    discrete element method

## References

1. Diniz, V.; Coiado, E.M. Two-phase (solid-liquid) flow in inclined pipes. In Proceedings of the 14th International Conference on Slurry Handling and Pipeline Transport, Maastricht, The Netherlands, 8–10 September 1999; Volume 36, pp. 555–566.
2. Juez, C.; Sandra, S.; Javier, M.; Pilar, G. Experimental and numerical simulation of bed load transport over steep slopes. *J. Hydraul. Res.* **2017**, *66*, 455–469. [[CrossRef](#)]
3. Li, Y.; Zhang, J.L.; Bai, Y.C.; Fu, J. Study on characteristics of sediment transport and sorting in pressure pipe. *J. Sediment Res.* **2021**, *46*, 10–15, 27.
4. Yue, J.W.; Huang, X.J.; Xing, X.X.; Zhao, L.M.; Kong, Q.M.; Yang, X.; Zhu, Y.D.; Zhang, J.W. Experimental Study on the Improvement of the Particle Gradation of the Yellow River Silt Based on MICP Technology. *Adv. Eng. Sci.* **2021**, *53*, 89–98.

5. Dabirian, R.; Mohan, R.; Shoham, O.; Kouba, G. Critical sand deposition velocity for gas-liquid stratified flow in horizontal pipes. *J. Nat. Gas Sci. Eng.* **2016**, *33*, 527–537. [[CrossRef](#)]
6. Shamlou, P.A. Hydraulic transport of particulate solids. *Chem. Eng. Commun.* **1987**, *62*, 233–249. [[CrossRef](#)]
7. Doron, P.; Barnea, D. Flow pattern maps for solid-liquid flow in pipes. *Int. J. Multiph. Flow* **1996**, *22*, 273–283. [[CrossRef](#)]
8. Gopaliya, M.; Kaushal, D.R. A Correlation for Pressure Drop Prediction for Solid-Liquid Slurry Flows through Horizontal Pipelines. *Multiph. Sci. Technol.* **2020**, *32*, 311–324. [[CrossRef](#)]
9. Skudarnov, P.V.; Lin, C.X.; Ebadian, M.A. Double-species slurry flow in a horizontal pipeline. *J. Fluids-Eng.-Trans. ASME* **2004**, *126*, 125–132. [[CrossRef](#)]
10. Soeptyan, F.B.; Cremaschi, S.; Sarica, C.; Subramani, H.J.; Kouba, G.E. Solids transport models comparison and fine-tuning for horizontal, low concentration flow in single-phase carrier fluid. *AICHE J.* **2014**, *60*, 76–122. [[CrossRef](#)]
11. Zhao, L.A.; Wang, T.L. Study on the flow of water sand slurry with sliding bed in inclined pipe. *J. Exp. Fluid Mech.* **2016**, *30*, 43–49.
12. Ogunesan, O.A.; Hossain, M.; Iyi, D.; Dhroubi, M.G. CFD Modelling of Pipe Erosion Due to Sand Transport. In Proceedings of the 1st International Conference on Numerical Modelling in Engineering, Ghent, Belgium, 28–29 August 2018; Springer: Singapore, 2019; pp. 274–289.
13. Pereira, G.C.; de Souza, F.J.; de Moro Martins, D.A. Numerical prediction of the erosion due to particles in elbows. *Powder Technol.* **2014**, *261*, 105–117. [[CrossRef](#)]
14. Mazumder, Q.H.; Shirazi, S.A.; Mclaury, B.S.; Shadley, J.R.; Rybicki, E.F. Development and validation of a mechanistic model to predict solid particle erosion in multiphase flow. *Wear* **2005**, *259*, 203–207. [[CrossRef](#)]
15. Ekambara, K.; Sanders, R.S.; Nandakumar, K.; Masliyah, J.H. Hydrodynamic Simulation of Horizontal Slurry Pipeline Flow Using ANSYS-CFX. *Ind. Eng. Chem. Res.* **2009**, *48*, 8159–8171. [[CrossRef](#)]
16. Kaushal, D.R.; Kaushal, D.R.; Tomita, Y.; Kuchii, S.; Tsukamoto, H. CFD modeling for pipeline flow of fine particles at high concentration. *Int. J. Multiph. Flow* **2012**, *43*, 85–100. [[CrossRef](#)]
17. Yang, Y.; Peng H.P.; Wen C. Sand Transport and Deposition Behaviour in Subsea Pipelines for Flow Assurance. *Energies* **2019**, *12*, 4070. [[CrossRef](#)]
18. Li, M.Z.; He, Y.P.; Liu, Y.D.; Huang, C. Analysis of transport properties with varying parameters of slurry in horizontal pipeline using ANSYS fluent. *Part. Sci. Technol.* **2020**, *38*, 726–739. [[CrossRef](#)]
19. Li, M.Z.; He, Y.P.; Liu, Y.D.; Huang, C. Hydrodynamic simulation of multi-sized high concentration slurry transport in pipelines. *Ocean. Eng.* **2018**, *163*, 691–705. [[CrossRef](#)]
20. Zhang, M.D.; Kang, Y.; Wei, W.; Li, D.; Xiong, T. CFD investigation of the flow characteristics of liquid-solid slurry in a large-diameter horizontal pipe. *Part. Sci. Technol.* **2021**, *39*, 712–725. [[CrossRef](#)]
21. Xiong, T.; Chen, Q.Y.; Wu, Q.; Zhang, M.D.; Wang, X. The numerical simulation on pipeline transport of coarse particles based on Eulerian-Lagrangian model. *Chin. J. Hydrodyn.* **2018**, *33*, 461–469.
22. Capecelatro, J.; Desjardins, O. An Euler-Lagrange strategy for simulating particle-laden flows. *J. Comput. Phys.* **2013**, *238*, 1–31. [[CrossRef](#)]
23. Zhang, Y.; Ren, W.L.; Li, P.; Zhang, X.H.; Lu, X.B. Flow regimes and characteristics of dense particulate flows with coarse particles in inclined pipe. *Powder Technol.* **2023**, *428*, 118859. [[CrossRef](#)]
24. Januario, J.R.; Maia, C.B. CFD-DEM Simulation to Predict the Critical Velocity of Slurry Flows. *J. Appl. Fluid Mech.* **2020**, *13*, 161–168. [[CrossRef](#)]
25. Liu, L.; Li, X.; Tian, X.L.; Zhang, X.T.; Xu, X.L.; Zhang, X.Z. Numerical Investigation on Inclined Hydraulic Transport of Large Particles for Deepsea Mining. *China Ocean Eng.* **2023**, *37*, 420–432. [[CrossRef](#)]
26. Kesely, M.; Matoušek, V.; Vlasak, P. Settling slurry flow near deposition velocity in inclined pipe of negative slope. *EPJ Web Conf.* **2019**, *213*, 02040. [[CrossRef](#)]
27. Matousek, V.; Kesely, M.; Vlasak, P. Modelling approaches for pipe inclination effect on deposition limit velocity of settling slurry flow. *EPJ Web Conf.* **2018**, *180*, 02062. [[CrossRef](#)]
28. Matousek, V.; Krupicka, J.; Kesely, M. A layered model for inclined pipe flow of settling slurry. *Powder Technol.* **2018**, *333*, 317–326. [[CrossRef](#)]
29. Matousek, V.; Kesely, M.; Konfrst, J.; Vlasak, P. Effect of pipe inclination on settling slurry flow near deposition velocity. *ASME Fluids Eng. Div. Meet.* **2018**, *3*, V003T19A008.
30. Vlasak, P.; Chara, Z.; Matousek, V.; Konfrst, J.; Kesely, M. Effect of pipe inclination on flow behaviour of fine-grained settling slurry. *EPJ Web Conf.* **2019**, *213*, 02094. [[CrossRef](#)]
31. Vlasak, P.; Chara, Z.; Matousek, V.; Konfrst, J.; Kesely, M. Experimental investigation of fine-grained settling slurry flow behaviour in inclined pipe sections. *J. Hydrol. Hydromech.* **2019**, *67*, 113–120. [[CrossRef](#)]
32. Archibong-Eso, A.; Aliyu, A.; Yan, W.; Okeke, N.; Baba, Y.; Fajemidu, O.; Yeung, H. Experimental Study on Sand Transport Characteristics in Horizontal and Inclined Two-Phase Solid-Liquid Pipe Flow. *J. Pipeline Syst. Eng. Pract.* **2020**, *11*, 04019050. [[CrossRef](#)]
33. Yang, D.; Xia, Y.M.; Wu, D.; Chen, P.; Zeng, G.Y.; Zhao, X.Q. Numerical investigation of pipeline transport characteristics of slurry shield under gravel stratum. *Tunn. Undergr. Space Technol.* **2018**, *71*, 223–230. [[CrossRef](#)]
34. Tebowei, R.; Hossain, M.; Islam, S.Z.; Dhroubi, M.G.; Oluyemi, G. Investigation of sand transport in an undulated pipe using computational fluid dynamics. *J. Pet. Sci. Eng.* **2018**, *162*, 747–762. [[CrossRef](#)]

35. Yao, R.; Qi, D.Z.; Zeng, H.Y.; Huang, X.X.; Li, B.; Wang, Y.; Bai, W.Q.; Wang, Z.W. Study on Critical Velocity of Sand Transport in V-Inclined Pipe Based on Numerical Simulation. *Water* **2022**, *14*, 2627. [[CrossRef](#)]
36. Alihosseini, M.; Thamsen, P.U. Analysis of sediment transport in sewer pipes using a coupled CFD-DEM model and experimental work. *Urban Water J.* **2019**, *16*, 259–268. [[CrossRef](#)]
37. Stevenson, P.; Thorpe, R.B.; Kennedy, J.E.; McDermott, C. The transport of particles at low loading in near-horizontal pipes by intermittent flow. *Chem. Eng. Sci.* **2001**, *56*, 2149–2159. [[CrossRef](#)]
38. Stevenson, P.; Thorpe, R.B.; Davidson, J.F. Incipient motion of a small particle in the viscous boundary layer at a pipe wall. *Chem. Eng. Sci.* **2002**, *57*, 4505–4520. [[CrossRef](#)]
39. Goharzadeh, A.; Rodgers, P.; Wang, L. Experimental Characterization of Slug Flow on Solid Particle Transport in a 1 Deg Upward Inclined Pipeline. *J. Fluids-Eng.-Trans. ASME* **2013**, *135*, 081304. [[CrossRef](#)]

**Disclaimer/Publisher’s Note:** The statements, opinions and data contained in all publications are solely those of the individual author(s) and contributor(s) and not of MDPI and/or the editor(s). MDPI and/or the editor(s) disclaim responsibility for any injury to people or property resulting from any ideas, methods, instructions or products referred to in the content.